SAG1.3-derived Frizzled-targeting negative allosteric modulators

Gunnar Schulte

gunnar.schulte@ki.se

Karolinska Institutet https://orcid.org/0000-0002-2700-7013

Lukas Grätz

Karolinska Institutet https://orcid.org/0000-0001-6755-0742

Ainoleena Turku

Karolinska Institutet https://orcid.org/0000-0003-0959-7221

Pawel Kozielewicz

Karolinska Institute https://orcid.org/0000-0003-1414-3566

Carl-Fredrik Bowin

Karolinska Institute https://orcid.org/0000-0001-9090-9493

Magdalena Scharf

Karolinska Institutet https://orcid.org/0000-0002-3305-3956

Jan Voss

Karolinska Institutet

Julia Kinsolving

Karolinska Institutet

Rawan Shekhani

Karolinska Institutet

Nuria Oliva-Vilarnau

Karolinska Institutet

Tobias Koolmeister

Karolinska Institutet

Marlies Körber

University of Erlangen-Nuremberg

Volker Lauschke

Karolinska Institutet https://orcid.org/0000-0002-1140-6204

Stefan Löber

University of Erlangen-Nuremberg

Peter Gmeiner

Universität Erlangen https://orcid.org/0000-0002-4127-197X

Article

Keywords:

Posted Date: February 20th, 2024

DOI: https://doi.org/10.21203/rs.3.rs-3910794/v1

Additional Declarations: Yes there is potential Competing Interest. Volker M Lauschke is co-founder, CEO and shareholder of HepaPredict AB, as well as co-founder and shareholder of PersoMedix AB. The other authors declare no conflict of interest.

SAG1.3-derived Frizzled-targeting negative allosteric modulators

Authors: Lukas Grätz[1,#], Ainoleena Turku[1,2,#], Pawel Kozielewicz[1], Carl-Fredrik Bowin[1,3], Magdalena M. Scharf[1], Jan H. Voss[1], Julia Kinsolving[1], Rawan Shekhani[1], Nuria Oliva-Vilarnau[4], Tobias Koolmeister[5], Marlies Körber[6], Volker M. Lauschke[4,7,8], Stefan Löber[6,9], Peter Gmeiner[6,9], Gunnar Schulte[1,*]

Affiliations:

[1]Karolinska Institutet, Dept. Physiology & Pharmacology, Sec. Receptor Biology & Signaling, Biomedicum, Stockholm, Sweden

[2]current address: Orion Pharma R&D, Espoo, Finland

[3]current address: University of Copenhagen, Department of Neuroscience, Copenhagen, Denmark

[4]Karolinska Institutet, Dept. Physiology & Pharmacology, Sec. Personalized Medicine and Drug Development, Biomedicum, Stockholm, Sweden

[5]Chemical Biology Consortium Sweden, Science for Life Laboratory, Department of Medical Biochemistry and Biophysics, Karolinska Institutet, Stockholm, Sweden

[6]Department of Chemistry and Pharmacy, Friedrich-Alexander-Universität Erlangen-Nürnberg, Erlangen, Germany

[7]Dr. Margarete Fischer-Bosch Institute of Clinical Pharmacology, Stuttgart, Germany

[8]University of Tübingen, Tübingen, Germany

[9]FAUNeW – Research Center New Bioactive Compounds, Friedrich-Alexander-Universität Erlangen-Nürnberg, Erlangen, Germany

[#] Authors contributed equally

*To whom correspondence should be addressed: gunnar.schulte@ki.se

Abstract:

Exaggerated Wingless/Int1 (WNT)/Frizzled (FZD) signaling contributes to pathologies including fibrosis and different forms of cancers. Thus, targeting FZDs as WNT receptors for therapeutic purposes constitutes a promising intervention if the imminent risk of unwanted side effects caused by the involvement of WNT/FZD signaling in stem cell regulation and tissue homeostasis can be controlled. Here, we derivatize SAG1.3, which acts through FZD_6 as a partial agonist. Screening of SAG1.3 derivates identified compound **11** that competed with BODIPY-cyclopamine binding at different FZDs and inhibited WNT-induced FZD dynamics and β-catenin signaling in HEK293 cells. Furthermore, compound **11** blocked WNT-3A-induced *Axin2* and *Lgr5* gene expression in human primary hepatocyte spheroids and reduced the viability of RNF43-mutated but not RNF43-wildtype pancreatic cancer cells. The small molecule acted as a paralog-nonselective negative allosteric modulator acting by limiting WNT- and WNT-surrogate induced receptor dynamics providing a valid proof-of-concept for targeting FZDs with small molecule compounds.

Introduction

The class Frizzled (class F) of G protein-coupled receptors consists of eleven receptors[1]. One of these receptors, Smoothened (SMO), mediates Hedgehog signaling and has already been targeted by an elaborate set of small molecule compounds, some of which are in clinical use for the treatment of basal cell carcinoma[2]. The other ten Frizzleds (FZD_{1-10}) bind the Wingless/Int-1 (WNT) family of secreted lipoglycoproteins via their extracellular cysteine-rich domain (CRD), which thereby represents by definition the orthosteric binding site of FZDs[3]. WNT/FZD signaling plays an essential role in embryonic development, stem cell regulation, tissue homeostasis and its perturbation. Imbalanced WNT/FZD signaling can result in diverse pathologies including various developmental disorders, fibrosis and cancer[4], making the WNT/FZD signaling system also a promising therapeutic target[5-9].

While some types of cancer, such as colon cancer, are often driven by WNT pathway mutations in genes encoding for proteins acting downstream of FZDs, such as mutations in APC (adenomatous polyposis coli) and β-catenin, other cancer types are associated with high expression levels of WNT proteins and increased total or surface expression of FZDs[5,9,10]. Therefore, it appears most suitable in the context of antitumor therapy to inhibit exaggerated WNT/FZD-mediated cell communication by developing inverse agonists, antagonists, or negative allosteric modulators into potential therapeutically meaningful concepts. Addressing cell surface receptors pharmacologically allows targeting signaling with higher precision especially when compared to modulation of downstream cascades that are often pleiotropically involved in complex signaling networks. In order to directly target FZDs, several strategies seem to be feasible. On one hand the route of targeting the orthosteric WNT binding site on the CRD by biologics such as antagonistic antibodies as well as bifunctional agonistic WNT mimetics, so

called WNT surrogates, has been pursued[11-14]. The CRD can also be targeted by small molecules exemplified by carbamazepine, which is surmised to block WNT-induced signaling at FZD_8[15]. On the other hand, following the more classical GPCR strategy, the seven transmembrane (7TM) core of FZDs offers diverse opportunities for drug targeting. Despite the claim that the core of FZDs could be undruggable[16], molecules can indeed target the FZD receptor core illustrated by the SMO agonist SAG1.3 that acts as a weak partial agonist at FZD_6[17]. Also, other core-targeting compounds have been identified by in silico structure-based virtual screening[18,19], and allosteric modulators acting at intracellular sites have been reported as folding chaperones with pharmacological activity[20,21].

Here, building on our previous efforts, we employ a strategy guided by a receptor model and systematic lead compound modifications to derivatize SAG1.3 aiming at the discovery of receptor core-targeting small molecules for FZDs. Competition binding experiments at FZD_6 enabled us to identify DJ503701 (compound **11)** as the compound with the highest affinity in our set. Further validation defined compound **11** as a negative allosteric modulator acting via the transmembrane core of FZDs in a paralog-nonselective manner, as it efficiently inhibited WNT-induced and FZD-mediated signaling in several diverse contexts including in HEK293 cells and patient-derived primary human liver spheroids. Furthermore, compound **11** reduced the viability of WNT-signaling-dependent human pancreatic ductal adenocarcinoma cells (PDAC). Thus, our findings demonstrate that FZDs indeed are druggable by small molecules and that negative allosteric modulation of FZD signaling can mediate therapy-relevant effects.

Results

Designing SAG1.3 analogues and ligand competition binding at FZD_6

We recently showed that the SMO agonist 1.3 (SAG1.3, see **Figure 1a**) acts on FZD_6 as a weak partial agonist by targeting the transmembrane receptor core[17,22]. However, SAG1.3 acts at FZD_6 with double-digit micromolar potency and very low efficacy, rendering it a relatively poor tool compound for studying FZD pharmacology effectively. Thus, we aimed at using the information about the binding site for the design of more potent FZD-targeting ligands. To do so, we divided SAG1.3 into three regions, which we called R^1-R^3 (see **Figure 1a**). Initially, we designed and synthesized a small number of SAG1.3 analogues (**1-24**) focusing on modifications of the R^3 region (**Figure 1a**) given that our receptor model suggested the availability of an aromatic sub-pocket able to accommodate such compounds (see **Supplementary Figure S1**). The compounds were tested at a concentration of 10 μM in a NanoBRET-based competition binding assay at Nluc-FZD_6 employing the tracer compound BODIPY-cyclopamine (**Figure 1b**), which we have previously used to assess FZD_6 binding in live HEK293 cells[17,22]. The chemical structures of all generated SAG1.3 analogues are shown in **Supplementary Table S1**. While some of the compounds were only weakly or not at all interfering with BODIPY-cyclopamine binding, others represented a significant improvement over the parent compound SAG1.3, almost reaching baseline levels ("donor only" control) at a concentration of 10 μM (**Figure 1c**, black dashed line). Building upon these first promising results, we set out to investigate the other two regions in SAG1.3 (R^1 and R^2), which had not been the focus in the first compound set. The design of the majority of analogues modified at R^1-R^3 was then based on exploring the chemical space which could be cost-effectively assessed both from an economical and chemical-synthetical perspective (compounds **25-59**). However, out of this second compound set, only a few showed better properties than the parental compound SAG1.3 (**Figure 1d**).

*Compound **11** binds non-selectively to the receptor core of FZDs*

Based on these screening results, twelve compounds were selected (cut-off value: 70% reduction of BODIPY-cyclopamine binding, see **Figure 1** and **Supplementary Table S1**) for full concentration-response curves in our competition binding assay setup. Interestingly, most of these compounds showed a sterically demanding substituent at the secondary amine. In particular, arylamide derivatives revealed very promising data. Confirming our screening results, all tested compounds were able to reduce tracer binding to Nluc-FZD_6 in a concentration-dependent manner (**Figure 2a**). The set of compounds displayed IC_{50} values in the low micromolar to high nanomolar range. DJ503701 (compound **11**, see **Figure 2b**) showed the highest pIC_{50} value (see **Figure 2a**, **Supplementary Figure S2** and **Supplementary Table S2**) and was therefore chosen for a more in-depth characterization. We performed analogous BODIPY-cyclopamine competition binding experiments with one member of every FZD homology cluster, employing ΔFZD_{1-10} HEK293 cells transiently transfected with N-terminally Nluc-tagged versions of either FZD_4, FZD_5 or FZD_7 to determine paralog selectivity. Compound **11** showed a similar ability to reduce BODIPY-cyclopamine binding from any of these receptors (see **Figure 2c** and **Supplementary Table S3**) suggesting that compound **11** is not selective within the FZD family. Competition binding experiments with a FZD_6 construct lacking the CRD (ΔCRD-Nluc-FZD_6) further support the notion – similar to what was observed for SAG1.3 – that compound **11** targets the transmembrane core of FZDs and not the orthosteric WNT binding site on the CRD (see **Figure 2d**).

*Definition of the mode of action of compound **11***

While SAG1.3 showed weak positive efficacy on FZD_6 with regard to conformational changes in the receptor core, miniG protein recruitment, heterotrimeric G_i protein activation, and extracellular signal-regulated kinases 1/2 phosphorylation, it remained unclear whether the positive efficacy of the parent compound was maintained through the chemical modification of the R^{1-3} moiety[17]. The ability of compound **11** to bind FZD paralogs non-selectively opened for a rich arsenal of functional assays to define the compound's mode of action. For this functional characterization, we decided to focus on human FZD_5, a receptor that mediates WNT-induced CRD dynamics, receptor core conformational changes, FZD-DVL interface dynamics, WNT/β-catenin signaling, and the activation of heterotrimeric G proteins[17,22-25]. In ΔFZD_{1-10} HEK293T cells transiently transfected with human FZD_5, addition of 300 ng/ml recombinant WNT-3A elicited a substantial TOPFlash response indicative of activation of the WNT/β-catenin pathway (**Figure 3a**). Compound **11** efficiently counteracted this WNT-3A-induced effect in a concentration-dependent manner with an pIC_{50} value of 5.92 ± 0.04 (equal to an IC_{50} value of 1.20 μM, **Figure 3b**) while not inducing any effect in the absence of added WNT-3A (see **Figure 3a**). In agreement with the BODIPY-cyclopamine competition binding experiments, compound **11** did not show a subtype preference in TOPFlash assays (see **Supplementary Figure S3**).

Initiation of WNT/β-catenin signaling is typically governed by WNT-mediated crosslinking of the extracellular regions of both FZD and the co-receptor LRP5/6 and the formation of a so-called signalosome. Signalosome formation can also be induced by artificial biologics called WNT surrogates carrying binding moieties for both entities[12]. Along these lines, addition of WNT surrogate to ΔFZD_{1-10} HEK293T cells transiently transfected with human FZD_5, led to a significant increase in WNT/β-catenin signaling (see **Figure 3c**). Notably, the WNT surrogate-

158 induced signal, only induced by cross-linking the extracellular moieties, could also be blocked
159 by co-addition of the core-binding small molecule compound **11** (see **Figure 3c**).

160 The phosphoprotein Dishevelled (DVL) is at the crossroads of both β-catenin-dependent and -
161 independent WNT signaling, and DVL interacts with FZDs mainly through its Dishevelled, Egl-
162 10 and pleckstrin (DEP) domain[24,26-28]. We have recently designed a genetically encoded
163 biosensor, which we called FZD_5-DEP-Clamp (for schematic depiction, see **Figure 3d**)[24],
164 selectively reporting on the WNT-induced FZD_5-DEP interface dynamics. WNT stimulation of
165 the FZD_5-DEP-Clamp sensor equipped with an intramolecular BRET donor-acceptor pair
166 displayed a robust increase in BRET (**Figure 3e**)[24]. In contrast, compound **11** alone did not elicit
167 a robust change in BRET response (see **Supplementary Figure S4**). However, in analogy to our
168 findings in the TOPFlash reporter gene assay, compound **11** was able to interfere with the WNT-
169 induced effects on the FZD_5-DEP-Clamp suggesting an information flow from the extracellular
170 WNT binding site to the intracellular FZD-DEP/DVL interface, which can be modulated by
171 small molecules binding to the receptor core in an allosteric manner.

172 Taken together, even though compound **11** binds to the receptor core and thus to a site distinct
173 from the orthosteric WNT binding site, the compound is still capable of impacting the signaling
174 output induced by WNT. Therefore, it acts by definition as a negative allosteric modulator
175 (NAM) of WNT/FZD-mediated signaling.

176

177 *NAMs can interfere with WNT-driven signaling in hepatocyte spheroids*

178 Next, we aimed to evaluate whether and how compound **11** would also impact signaling in a
179 physiologically relevant, non-recombinant system. To this end, we used organotypic 3D cultures

of primary human hepatocytes (PHH) in which the cultured cells retain their transcriptomic, proteomic and metabolomic phenotype for multiple weeks[29-31].

The liver is the organ with the highest regenerative capacity in the human body, for which functional WNT/β-catenin signaling among other pathways is a critical cue[32]. To assess the effects of compound **11**, we generated 3D spheroids from primary human hepatocytes (PHH) and monitored expression changes of the two prototypical WNT/β-catenin target genes *Axin2* and *Lgr5* upon addition of WNT alone or together with the non-FZD-selective NAM compound **11**. In agreement with previous reports, addition of WNT-3A increased the mRNA levels of *Axin2* and especially *Lgr5* (see **Figure 4a**)[33]. Upon co-addition of compound **11**, a reduction of the WNT-induced increase in expression could be detected for both target genes returning mRNA expression almost back to vehicle levels. Even though statistical significance was only reached for *Lgr5*, the same trend was observed for *Axin2*. This observation confirmed that compound **11** interferes with WNT/β-catenin signaling also in more complex and physiologically relevant test systems.

FZD NAM reduces viability of RNF43-negative pancreatic cancer cells

The development of small molecules directly inhibiting FZD function represents an interesting yet unexploited avenue for drug discovery and therapy, even though some improvements have been made. Inhibition of FZDs could have a therapeutical benefit for tumor subtypes that are driven by either overexpression of WNTs, activating mutations of FZDs or enhanced cell surface expression of FZDs. In human pancreatic ductal adenocarcinoma (PDAC), about 7% of the patients present with impairing mutations in the E3 ubiquitin ligase RNF43, which was described

to reduce surface levels of FZDs[34]. The interrupted inhibitory regulation by RNF43 of FZD surface expression results in an enhanced autocrine WNT-dependent signaling loop[9,35]. It was further shown that disruption of this signaling axis in this RNF43-negative subgroup of PDAC cell lines through pharmacological inhibition of the O-acyltransferase porcupine, which is essential for WNT secretion, led to reduced cell proliferation suggesting that their survival depends on a functional WNT/FZD signaling axis (**Figure 4b**, top panel)[9,35-37]. Building upon these reports, we therefore hypothesized an alternative potential interference strategy: addressing the WNT/FZD signaling axis directly on the receptor level through a FZD-targeting NAM such as compound **11** should also reduce the viability of RNF43-negative and thus WNT-sensitive pancreatic cancer cells. Indeed, cell viability of RNF43-negative HPAF-II cells was strongly reduced upon treatment with compound **11** (see **Figure 4b** and **Supplementary Figure S5**). In contrast, PANC-1 cells, which do not carry an inactivating mutation in RNF43 and whose survival therefore does not depend on a functioning autocrine WNT signaling loop, were not significantly affected. These results provide further evidence that FZD-targeting small molecules indeed provide a therapeutic opportunity in cancer types stratified for WNT dependence that is caused for example by RNF43 mutations but potentially also overexpression of WNTs or FZDs.

Discussion

Here, we report on the development of a NAM targeting FZDs in a paralog-non-selective manner. Derivatizing SAG1.3 has resulted in the discovery of DJ503701 (compound **11**), which was not only able to efficiently suppress WNT/β-catenin signaling in HEK293 cells but also in hepatocyte-derived spheroids. Moreover, compound **11** reduced the survival of WNT signaling-dependent pancreatic cancer cells thereby opening new therapeutic avenues.

The starting point of our study was the SMO agonist or FZD_6 weak partial agonist SAG1.3, which was divided into three regions (R^1-R^3, see **Figure 1a**). SAG1.3 derivatives modified in one or more regions were synthesized and screened for binding to FZD_6. It was evident from the screening results that ten of the twelve compounds selected for further characterization were only modified in R^3 compared to only two that were modified in other regions. Full concentration-response curves in competition binding experiments at Nluc-FZD_6 revealed compound **11** as the one with the highest potency in our set exhibiting IC_{50} values in the three-digit nanomolar to single-digit micromolar range, while not showing subtype selectivity within the FZD family (see **Figure 2c**). Being based on SAG1.3 and supported by binding experiments using a FZD_6 construct lacking the extracellular region (ΔCRD-Nluc-FZD_6, see **Figure 2d**), we propose that compound **11** binds to the transmembrane region rather than the orthosteric WNT binding site, the CRD.

A functional characterization using readouts for WNT/β-catenin signaling and the dynamic changes in the FZD_5-DEP interface defined compound **11** as a NAM of WNT-induced and FZD-mediated effects without possessing any intrinsic efficacy on FZDs (see **Figure 3**). This observation could be confirmed in PHH-derived spheroids as an example for a more complex cell model, in which compound **11** was able to suppress WNT-induced target gene transcription close to basal levels (see **Figure 4**). Compound **11** was moreover capable of reducing the viability of a specific group of RNF43-mutated pancreatic cancer cells (e.g., HPAF-II), whose survival is dependent on functional WNT signaling[9,35]. This can serve as a proof-of-concept of allosteric modulation of FZDs in a therapeutically relevant context substantially expanding the concept of targeting FZDs with CRD-binding biologics in the same experimental model[9].

Currently, several paradigms coexist explaining the mechanisms underlying WNT signal initiation and pathway specification. One of them is the signalosome model, according to which the initiation of WNT signaling is achieved by WNTs serving as crosslinkers between FZDs and certain co-receptors, e.g., LRP5/6 for WNT/β-catenin signaling thereby specifying the signaling outcome[38,39]. While the signalosome model excludes intrinsic receptor dynamics[40-42], FZDs behave – in agreement with what is known for other GPCRs – as dynamic entities, sometimes referred to as molecular machines[24,43,44]. The latter model includes an allosteric coupling between the CRD – the orthosteric WNT binding site – and the intracellular transducer coupling interface[23,24,45,46]. Without contradicting the necessity and relevance of co-receptors, the ability of the NAM to block WNT- and especially WNT surrogate-induced β-catenin signaling, emphasizes that the CRD and the receptor core are allosterically interconnected and cooperate to initiate WNT signaling. A model that explains signal initiation solely by complexing a signalosome in the absence of FZD dynamics cannot explain the negative allosteric modulation of WNT signaling by a NAM. Thus, our findings underline the need to integrate the signalosome model with functional FZD dynamics to fully understand how WNT signaling is initiated and specified.

Previous efforts of targeting FZDs pharmacologically resulted in diverse biologics targeting the CRD and various small molecules addressing mainly the receptor core. WNT surrogates were developed based on the signalosome concept as WNT mimics by crosslinking FZDs and LRP5/6 eventually inducing WNT/β-catenin signaling[11,12]. While the development of WNT surrogates undoubtedly presents an exciting opportunity for applications in regenerative medicine,

promoting for example alveolar regeneration after injury[8], their positive efficacy limits their use in the treatment of diseases presenting with overactive WNT signaling, e.g., certain types of cancer. To fill this gap, other biomolecules including peptides, antibodies, or antibody fragments were investigated, which block WNT binding to the CRD of FZDs[9,14,47-49]. Many of the developed antibodies showed promising effects on tumor growth and in in-vitro studies. Most prominently, vantictumab, a monoclonal antibody binding to five of ten FZD paralogs even made it to Phase Ib clinical trials until being dismissed due to bone toxicity[13,50].

As an alternative strategy, there were a few reports over the last years on small organic compounds binding to the transmembrane core of FZDs even though this region of the receptors was deemed undruggable[16]. Some of these compounds were even capable of suppressing WNT signaling but the mechanisms of action of these compounds were poorly defined[18,19].

In the present study, we further extend the concept of the modulation of WNT signaling with small molecules by targeting the 7TM core instead of directly interfering with WNT binding. We foresee that this strategy can indeed present a valid direction for future FZD-directed drug discovery. By definition, receptors only possess one orthosteric binding site while having many more allosteric binding pockets, which increases the number of potentially targetable sites[51]. Moreover, it is a hallmark of allosteric modulators (without intrinsic efficacy) that they only affect receptor signaling in the presence of the respective orthosteric ligand, thus “fine-tuning” its response[52]. With respect to eventually using drugs targeting the WNT/FZD signaling axis in a clinical setting, we envision that modulating or tuning the WNT response instead of interfering with WNT binding and thus completely blocking signaling, e.g., as done with CRD-targeting

antibodies, might be advantageous in terms of the drug safety profile, especially in a paralog- and eventually pathway-selective manner.

The characterization of FZD-targeting NAMs does not only provide useful tool compounds but also deeper insight into FZD activation mechanisms and dynamics. The series of SAG1.3 derivatives presents a conceptual starting point for further refinement and discovery of compounds with higher affinity and potentially FZD paralog selectivity. Achieving paralog selectivity can be instrumental to find a window of opportunity for human therapy balancing therapeutic and undesired on-target side effects in FZD-targeting therapeutic approaches.

Online Methods

Cell culture and transfection

Human embryonic kidney cells (HEK293A, female origin, Thermo Fisher Scientific), ΔFZD_{1-10} HEK293T cells (kindly provided by Benoit Vanhollebeke)[53], ΔSMO HEK293A cells[54] and the pancreatic cancer cell lines HPAF-II (American Tissue Culture Collection (ATCC)) and PANC-1 (ATCC) were routinely cultured in complete Dulbecco's Modified Eagle's Medium (DMEM, Hyclone), supplemented with 1% penicillin/streptomycin (Gibco, #151-40122) and 10% fetal bovine serum (FBS, Gibco) in a humidified 5% CO_2 incubator at 37 °C. All used cell culture plastics were purchased from Sarstedt or VWR, unless specified otherwise. Whenever indicated, cells were transiently transfected in suspension with 1 µg of total plasmid DNA per mL cell suspension using either Lipofectamine 2000 (Invitrogen, Lipofectamine (µL): DNA (µg) = 2:1) or linear polyethyleneimine (PEI, Alfa Aesar, MW 25,000, stock solution: 1 mg/mL; PEI (µL): DNA (µg) = 5:1) as the transfection reagents. All transfected plasmid amounts indicated below refer to the amount of plasmid DNA used to transfect 1 mL of cell suspension.

The absence of mycoplasma contamination was routinely confirmed by polymerase chain reaction using 5′-GGC GAA TGG GTG AGT AAC ACG-3′ (forward) and 5′-CGG ATA ACG CTT GCG ACT ATG-3′ (reverse) primers, which were designed to detect 16S ribosomal RNA of mycoplasma in the media after at least 3 days of cell exposure.

Plasmids and stable cell line generation

Plasmids encoding HiBiT-FZD_4, HiBiT-FZD_5, HiBiT-FZD_7, HiBiT-FZD_8, Nluc-FZD_4 and Nluc-FZD_6 have been described previously[55,56]. Plasmids encoding Nluc-FZD_5 and Nluc-FZD_7 were

generated by replacing the FZD_4 sequence in the Nluc-FZD_4 backbone with the respective nucleotide sequences for FZD_5 and FZD_7 via the *BamH*I and *Xba*I restriction sites in HiBiT-FZD_5 and HiBiT-FZD_7[55]. ΔCRD-Nluc-FZD_6 was cloned by amplifying ΔCRD-FZD_6 (starting from D156) using SNAP-FZD_6 as a template (kind gift from Madelon M. Maurice (University Medical Center Utrecht, Utrecht, The Netherlands)). The amplicon was then also cloned into the Nluc-FZD_4 backbone using *BamH*I and *Xba*I restriction sites. To generate the FZD_5-DEP-Clamp (TK) plasmid, which was used to generate the stable FZD_5-DEP-Clamp HEK293A cell line, the sequence for the human thymidine kinase promoter (TK, note: weak promoter sequence) was amplified from pRL-TK (Promega, E2241) and used to replace the CMV promoter present in the original FZD_5-DEP-Clamp plasmid[24] via Gibson assembly. The Super 8X TOPFlash plasmid was obtained from Addgene (#12456) and the Renilla luciferase control plasmid pRL-TK was from Promega.

Primer sequences used to generate new plasmids are listed in **Supplementary Table S4**. Sequences of all newly generated plasmids were verified by Sanger sequencing (Eurofins Genomics).

To generate the stable FZD_5-DEP-Clamp cell line, HEK293A cells were seeded at a density of 500,000 cells/well in a 6-well plate. On the next day, the adherent cells were transfected with 2 µg of FZD_5-DEP-Clamp (TK) plasmid using PEI as the transfection reagent. After two days of transfection, cells were detached and transferred to a 75 cm^2 flask. Stably transfected cells were selected using complete medium (DMEM + 10% FCS + 1% penicillin/streptomycin) supplemented with 2000 µg/mL G-418 sulfate (Gibco, cat.-No.:10131027) for three weeks. After obtaining stable growth, cell culture of the stable cell line was continued with 500 µg/mL G-418.

Primary human hepatocyte cell culture

Cryopreserved adult primary human hepatocytes (PHH) were purchased from BioIVT (USA) and cultured as 3D spheroids as previously described[31]. Briefly, PHH were seeded in 96-well ultra-low attachment plates (Corning) at a density of 1500 cells/well in William's E medium (Gibco) supplemented with insulin, transferrin, and selenium (ITS, Life technologies), 100nM dexamethasone (Sigma) and 10% fetal bovine serum (Cytiva). PHH were treated from start of the culture with vehicle control (DMSO), recombinant WNT-3A and 10µM compound **11** for 48 h, as indicated. The supplier BioIVT collected informed consent from each donor or the subject's legally authorized representative and the documentation was reviewed and approved by the appropriate regulatory authorities in accordance with HHS regulations for the protection of human subjects (45 CFR §46.116 and §46.117) and Good Clinical Practice (ICH E6). The demographics and medical history of the donor used are reported in **Supplementary Table S5**.

Ligands

Synthesis procedures for compounds selected for further characterization after the first screen (**9**, **10**, **11**, **14**, **15**, **17**, **18**, **19**, **21**, **23**, **24**, **52**) incl. the respective analytical characterization can be found in the Supplementary Information. Stock solutions of all newly synthesized small molecules were prepared in pure DMSO at a concentration of 10 mM. SAG1.3 (IUPAC: 3-chloro-N-[trans-4-(methylamino)cyclohexyl]-N-[[3-(4-pyridinyl)phenyl]methyl]-benzo[b]thiophene-2-carboxamide dihydrochloride) was purchased from Sigma-Aldrich (cat.-No.: SML1314) and dissolved at a concentration of 10 mM in Millipore water. BODIPY-cyclopamine (BioVision, cat.-No.: 2160) was dissolved at 1 mM in DMSO and stored in

aliquots. The porcupine inhibitor C59 (IUPAC: 2-[4-(2-Methylpyridin-4-yl)phenyl]-N-[4-(pyridin-3-yl)phenyl]acetamide, Abcam, cat.-No.: ab142216) was dissolved at 10 mM in DMSO and used wherever indicated to reduce endogenous WNT secretion. All stock solutions of small molecule compounds were stored at -20 °C.

Lyophilized recombinant WNT-3A (R&D Systems, 5036-WN-010) and high-purity WNT-3A (R&D Systems, 5036-WNP-010) were resuspended in 0.1% bovine serum albumin (BSA, Sigma Aldrich)/Dulbecco's phosphate-buffered saline (DPBS, Hyclone) at a concentration of 100 µg/mL or 200 µg/mL, respectively. WNT-surrogate-Fc fusion protein (WNT surrogate, U-Protein Express B.V., cat.-No.: N001) was diluted to a concentration of 500 nM with 0.1% BSA/DPBS. WNT-3A and WNT surrogate stock solutions were stored at 4 to 8 °C for a maximum of six weeks.

BRET-based binding assays

One day prior the experiment, ΔFZD_{1-10} HEK293T (400,000 cells/mL) or ΔSMO HEK293A cells (300,000 cells/mL) were transiently transfected in suspension with 10 ng of Nluc-FZD_x and 990 ng of empty pcDNA3.1 (to adjust the DNA amount) per mL cell suspension and seeded (ΔFZD_{1-10} HEK293T cells: 40,000 cells/well, ΔSMO HEK293A cells: 30,000 cells/well) in poly-D-lysine (PDL)-coated, white opaque 96-well plates (Nunc, Thermo Fisher Scientific). After 24 h, cells were washed once with HBSS, followed by the addition of 80 µL of HBSS. Next, 10 µL of the competitive ligand, i.e., the tested SAG1.3 derivative (either in different concentrations for the concentration-response curves or at a final concentration of 10 µM for the first screens), and 10 µL of the fluorescent tracer BODIPY-cyclopamine (final concentration: 300 nM for the first

screens, 200 nM for the concentration-response experiments) were added. All serial dilutions were prepared in HBSS. The cells were incubated for 90 min at 37 °C without additional CO_2, after which 10 µL of luciferase substrate diluted in HBSS (furimazine (Promega, N1572), final dilution: 1:1000 for first screening; coelenterazine h (Biosynth, final concentration: 5 µM) for concentration-response experiments) were added to the cells. Following a 10 min incubation period in the dark, the measurement was started on a BMG Labtech ClarioStar or TECAN Spark multimode microplate reader, prewarmed to 37 °C. Nluc bioluminescence was detected between 460 and 490 nm (ClarioStar) or 460 and 500 nm (TECAN Spark). The emission of the fluorescent tracer was detected between 520 and 550 nm (ClarioStar) or between 520 and 560 nm (TECAN Spark).

TOPFlash reporter gene assay

ΔFZD_{1-10} HEK293T cells were transiently transfected in suspension (450,000 cells/mL) with a mix of 200 ng of HiBiT-FZD_x (paralog indicated in figures), 250 ng of Super 8X TOPFlash reporter (TCF/LEF-activity-dependent Firefly luciferase (Fluc) expression), 75 ng of pRL-TK (constitutive Renilla luciferase (Rluc) expression as a transfection control) and 475 ng of empty pcDNA3.1 (to adjust the DNA amount) per mL cell suspension (450,000 cells/mL). The transfected cell suspension was then seeded (45,000 cells/well) in a PDL-coated, white opaque 96-well plate. One day after transfection, cells were washed once with HBSS and 80 µL of serum-free DMEM containing 10 nM of the porcupine inhibitor C59 were added. Next, 10 µL of compound **11** (concentrations as indicated) or DMSO were added, followed by the addition of 10 µL of recombinant WNT-3A (final concentration: 300 ng/mL), WNT surrogate (final concentration: 250 pM) or their respective vehicle controls. All ligands/vehicle controls were

diluted in serum-free DMEM containing 10 nM C59. One day after ligand stimulation, cells were washed once with HBSS and the lysis was started using 1X Passive Lysis Buffer (Promega, cat.-No.: E1910, 20 µL/well), after which the plate was shaken for 20 min at room temperature. Fluc and Rluc bioluminescence were then assessed using the Dual-Luciferase Assay System (Promega, cat.-No.: E1910, 20 µL of both LARII (Luciferase Assay II reagent) and 1X Stop-and-Glo Reagent). Measurements were performed using a TECAN Spark multi-mode microplate reader. Fluc bioluminescence (proportional to the activation of β-catenin-dependent gene transcription) was detected between 550 and 620 nm (integration time: 2000 ms), while Rluc bioluminescence (constitutive transfection control measure) was measured between 445 and 530 nm (integration time: 2000 ms).

Gene expression analysis in primary hepatocytes

RNA from 24 hepatocyte spheroids per condition was isolated using Qiazol lysis reagent (QIAGEN). For expression profiling of target genes by qPCR, cDNA synthesis was carried out using SuperScript III reverse transcriptase (Invitrogen) and expression was evaluated using Taqman probes (**Supplementary Table S6**) according to supplier's instructions in a 7500 Fast Real-Time PCR system (Applied Biosystems). Gene expression was quantified using the $\Delta\Delta Ct$ method (normalized to the average of the vehicle control from all three experiments).

Cell viability

HPAF-II cells and PANC-1 cells were seeded in DMEM at a density of 1000 cells per well in a black opaque 96-well plate (Greiner BioOne). After one day, the medium was exchanged with

complete DMEM containing either compound **11**, the porcupine inhibitor C59 or DMSO (vehicle control). After three days of incubation (37 °C, 5% CO_2), the medium was exchanged once again with DMEM containing the same concentration of ligands or DMSO (vehicle control). Three days after (equal to seven days after seeding), the medium was removed and 90 µL of fresh DMEM (without any ligands) were added. Lastly, 10 µL of AlamarBlue HS reagent (Thermo Fisher Scientific, cat.-No.: A50100) were added to each well and the cells were incubated for 4 h at 37 °C inside the incubator (5% CO_2). After the incubation step, fluorescence was read using a TECAN Spark multi-mode microplate reader (excitation: 535 ± 25 nm, emission: 595 ± 35 nm).

Receptor modelling

In the compound design focusing on R^3 modifications, we utilized FZD_6 models as previously described[17]. The model, where the docked SAG1.3 pose was in the best agreement with the SAG1.5 pose in the SMO-SAG1.5 crystal structure (PDB ID: 4QIN) was selected for the docking studies[57]. Docking was performed with Autodock Vina 1.1.2 and SAG1.3 defined the location of the utilized docking grid. Ten poses per compound were written out, and they underwent visual analysis by which the most promising designs were selected for synthesis.

Data and statistical analysis

All raw data from plate reader experiments were obtained as Microsoft Excel spreadsheets. The subsequent data analysis and visualization was performed in Microsoft Excel and GraphPad Prism 9.0.

BRET was defined as the ratio of acceptor emission (BODIPY-cyclopamine/mVenus-tagged protein) over the donor emission (Nluc-tagged protein).

For each binding experiment, the measurement was repeated five times and averaged for the analysis. ΔBRET values were obtained by subtracting the BRET ratio obtained in wells containing BODIPY-cyclopamine but no competitive ligand (100% value. The BRET values for full displacement were defined using "donor only" control wells, which contained Nluc-FZD_x-transfected cells but no BODIPY-cyclopamine.

For the full concentration-response BRET binding curves in **Figure 2**, BRET values were normalized (separately for each experiment) to control wells containing BODIPY-cyclopamine but no competitive ligand (100% value) and "donor only" wells (0% value, described above). The normalized data were analyzed using three-parameter or four-parameter nonlinear regression, where the model was chosen for each independent experiment separately after running extra-sum-of-squares F-tests ($p < 0.05$) resulting in an IC_{50} value. Obtained IC_{50} values were transformed to pIC_{50} values, which were subsequently averaged between experiments. Displacement curves showing the non-normalized data (ΔBRET values generated as described above) can be found in **Supplementary Figure S2**.

For reporter gene assays, the TOPFlash ratio was defined as the ratio of β-catenin-dependent gene transcription (Firefly luciferase) over a constitutively expressed transfection control (Renilla luciferase). For all experiments, the calculated TOPFlash ratios were normalized to the respective vehicle conditions. For the concentration-response curve of compound **11** (**Figure 2b**), the vehicle-corrected TOPFlash ratios were normalized (100% value) to the wells containing WNT-3A but no compound **11**.

For kinetic experiments with the FZD_5-DEP-Clamp sensor, BRET values were first baseline-corrected for every well separately by subtracting the average of the first three reads prior ligand addition. Afterwards, the average values for vehicle-containing wells were subtracted for every timepoint to get access to actual ligand-induced changes in BRET ratio (ΔBRET values).

For the WNT target gene analysis in PHH-derived spheroids, $\Delta\Delta Ct$ values were calculated by normalization to the averaged vehicle control from three independent experiments.

For each cell viability experiment, the fluorescence measured in ligand-treated wells was normalized to the fluorescence from wells treated with vehicle control (DMSO).

Statistical significance was assessed using either one-way analysis of variance (ANOVA) or two-way ANOVA. In all instances, $p < 0.05$ was considered significant. Specific details are given in the respective figure legends.

Acknowledgments: We thank Benoit Vanhollebeke for the ΔFZD_{1-10} HEK293 cells. The work was supported by grants from Karolinska Institutet, the Swedish Research Council (GS: 2017-04676, 2019-01190; VML: 2019-01837, 2021-02801, 2023-03015; PK: 2022-01398), the Swedish Cancer Society (GS: CAN2017/561, 20 1102 PjF, 23 2825 Pj; PK: 20 0264P), the Swedish Society for Medical Research (PK: P19-0055; MMS: PG-22-0379-H-01), the Novo Nordisk Foundation (GS: NNF17OC0026940, NNF20OC0063168, NNF21OC0070008, NNF22OC0078104), The German Research Foundation (DFG; LG: 504098926; MMS: 470002134; JHV: 520506488), Wenner-Gren Foundations (UPD2018-0064), Emil and Wera Cornells Stiftelse, Alex och Eva Wallström Stiftelse (PK: 2020-00228) and Stiftelsen Lars Hiertas Minne (PK: FO2019-0086, FO2020-0304, FO2021-0127). This project has received

funding from the Innovative Medicines Initiative 2 Joint Undertaking (JU) under grant agreement No 875510. The JU receives support from the European Union's Horizon 2020 research and innovation programme and EFPIA and Ontario Institute for Cancer Research, Royal Institution for the Advancement of Learning McGill University, Kungliga Tekniska Högskolan, Diamond Light Source Limited.

Author contributions:

Conceived the project: GS, AT, PK

Synthesized compounds: TK, MK, SL, PG

Performed wet lab experiments: LG, CFB, PK, JHV, RS, JK

Analyzed data: PK, LG, CFB, AT

Protein modelling and docking: AT, MMS

Performed experiments and provided data on spheroids: NV, VML

Wrote the manuscript and prepared the figures: AT, LG, GS, MMS

Contributed to writing: PK, SL, TK

Supervised the project: GS

Competing interests: VML is co-founder, CEO and shareholder of HepaPredict AB, as well as co-founder and shareholder of PersoMedix AB. The other authors declare no conflict of interest.

Data and materials availability: Data supporting the findings of this manuscript are available from the corresponding author upon reasonable request. A reporting summary for this article is available as a Supplementary Information file. Expression vectors used and created for this work can be obtained from corresponding author.

References

1 Schulte, G. International Union of Basic and Clinical Pharmacology. LXXX. The class Frizzled receptors. *Pharmacological reviews* **62**, 632-667, doi:10.1124/pr.110.002931 (2010).

2 Teglund, S. & Toftgard, R. Hedgehog beyond medulloblastoma and basal cell carcinoma. *Biochimica et biophysica acta* **1805**, 181-208, doi:10.1016/j.bbcan.2010.01.003 (2010).

3 Janda, C. Y., Waghray, D., Levin, A. M., Thomas, C. & Garcia, K. C. Structural basis of Wnt recognition by Frizzled. *Science* **337**, 59-64, doi:10.1126/science.1222879 (2012).

4 Steinhart, Z. & Angers, S. Wnt signaling in development and tissue homeostasis. *Development* **145**, doi:10.1242/dev.146589 (2018).

5 Larasati, Y., Boudou, C., Koval, A. & Katanaev, V. L. Unlocking the Wnt pathway: Therapeutic potential of selective targeting FZD7 in cancer. *Drug discovery today* **27**, 777-792, doi:10.1016/j.drudis.2021.12.008 (2022).

6 Flanagan, D. J., Vincan, E. & Phesse, T. J. Winding back Wnt signalling: potential therapeutic targets for treating gastric cancers. *Br J Pharmacol*, doi:10.1111/bph.13890 (2017).

7 Blagodatski, A., Poteryaev, D. & Katanaev, V. L. Targeting the Wnt pathways for therapies. *Molecular and cellular therapies* **2**, 28, doi:10.1186/2052-8426-2-28 (2014).

8 Nabhan, A. N. *et al.* Targeted alveolar regeneration with Frizzled-specific agonists. *Cell* **186**, 2995-3012 e2915, doi:10.1016/j.cell.2023.05.022 (2023).

9 Steinhart, Z. *et al.* Genome-wide CRISPR screens reveal a Wnt-FZD5 signaling circuit as a druggable vulnerability of RNF43-mutant pancreatic tumors. *Nature medicine* **23**, 60-68, doi:10.1038/nm.4219 (2017).

10 Yu, J. *et al.* The Functional Landscape of Patient-Derived RNF43 Mutations Predicts Sensitivity to Wnt Inhibition. *Cancer research* **80**, 5619-5632, doi:10.1158/0008-5472.CAN-20-0957 (2020).

11 Miao, Y. *et al.* Next-Generation Surrogate Wnts Support Organoid Growth and Deconvolute Frizzled Pleiotropy In Vivo. *Cell stem cell* **27**, 840-851 e846, doi:10.1016/j.stem.2020.07.020 (2020).

12 Janda, C. Y. *et al.* Surrogate Wnt agonists that phenocopy canonical Wnt and beta-catenin signalling. *Nature* **545**, 234-237, doi:10.1038/nature22306 (2017).

13 Davis, S. L. *et al.* A phase 1b dose escalation study of Wnt pathway inhibitor vantictumab in combination with nab-paclitaxel and gemcitabine in patients with previously untreated metastatic pancreatic cancer. *Invest New Drugs* **38**, 821-830, doi:10.1007/s10637-019-00824-1 (2020).

14 Gurney, A. *et al.* Wnt pathway inhibition via the targeting of Frizzled receptors results in decreased growth and tumorigenicity of human tumors. *Proc Natl Acad Sci U S A* **109**, 11717-11722, doi:10.1073/pnas.1120068109 (2012).

15 Zhao, Y., Ren, J., Hillier, J., Lu, W. & Jones, E. Y. Antiepileptic Drug Carbamazepine Binds to a Novel Pocket on the Wnt Receptor Frizzled-8. *J Med Chem* **63**, 3252-3260, doi:10.1021/acs.jmedchem.9b02020 (2020).

16 Yang, S. *et al.* Crystal structure of the Frizzled 4 receptor in a ligand-free state. *Nature* **560**, 666-670, doi:10.1038/s41586-018-0447-x (2018).

17 Kozielewicz, P. *et al.* Structural insight into small molecule action on Frizzleds. *Nat Commun* **11**, 414, doi:10.1038/s41467-019-14149-3 (2020).

18 Zhang, W., Lu, W., Ananthan, S., Suto, M. J. & Li, Y. Discovery of novel frizzled-7 inhibitors by targeting the receptor's transmembrane domain. *Oncotarget* **8**, 91459-91470, doi:10.18632/oncotarget.20665 (2017).

19 Li, C. *et al.* Structure-Based Ligand Discovery Targeting the Transmembrane Domain of Frizzled Receptor FZD7. *J Med Chem* **66**, 11855-11868, doi:10.1021/acs.jmedchem.2c01795 (2023).

20 Generoso, S. F. *et al.* Pharmacological folding chaperones act as allosteric ligands of Frizzled4. *Nat Chem Biol* **11**, 280-286, doi:10.1038/nchembio.1770 (2015).

21 Riccio, G. *et al.* A Negative Allosteric Modulator of WNT Receptor Frizzled 4 Switches into an Allosteric Agonist. *Biochemistry* **57**, 839-851, doi:10.1021/acs.biochem.7b01087 (2018).

22 Turku, A., Schihada, H., Kozielewicz, P., Bowin, C. F. & Schulte, G. Residue 6.43 defines receptor function in class F GPCRs. *Nat Commun* **12**, 3919, doi:10.1038/s41467-021-24004-z (2021).

23 Wright, S. C. *et al.* A conserved molecular switch in Class F receptors regulates receptor activation and pathway selection. *Nat Commun* **10**, 667, doi:10.1038/s41467-019-08630-2 (2019).

24 Bowin, C. F. *et al.* WNT stimulation induces dynamic conformational changes in the Frizzled-Dishevelled interaction. *Sci Signal* **16**, eabo4974, doi:10.1126/scisignal.abo4974 (2023).

25 Gratz, L. *et al.* NanoBiT- and NanoBiT/BRET-based assays allow the analysis of binding kinetics of WNT-3A to endogenous Frizzled 7 in a colorectal cancer model. *Br J Pharmacol*, doi:10.1111/bph.16090 (2023).

26 Gao, C. & Chen, Y. G. Dishevelled: The hub of Wnt signaling. *Cellular signalling* **22**, 717-727, doi:10.1016/j.cellsig.2009.11.021 (2010).

27 Gammons, M. V., Renko, M., Johnson, C. M., Rutherford, T. J. & Bienz, M. Wnt Signalosome Assembly by DEP Domain Swapping of Dishevelled. *Molecular cell* **64**, 92-104, doi:10.1016/j.molcel.2016.08.026 (2016).

28 Tauriello, D. V. *et al.* Wnt/beta-catenin signaling requires interaction of the Dishevelled DEP domain and C terminus with a discontinuous motif in Frizzled. *Proc Natl Acad Sci U S A* **109**, E812-820, doi:10.1073/pnas.1114802109 (2012).

29 Bell, C. C. *et al.* Transcriptional, Functional, and Mechanistic Comparisons of Stem Cell-Derived Hepatocytes, HepaRG Cells, and Three-Dimensional Human Hepatocyte Spheroids as Predictive In Vitro Systems for Drug-Induced Liver Injury. *Drug Metab Dispos* **45**, 419-429, doi:10.1124/dmd.116.074369 (2017).

30 Vorrink, S. U. *et al.* Endogenous and xenobiotic metabolic stability of primary human hepatocytes in long-term 3D spheroid cultures revealed by a combination of targeted and untargeted metabolomics. *Faseb J* **31**, 2696-2708, doi:10.1096/fj.201601375R (2017).

31 Bell, C. C. *et al.* Characterization of primary human hepatocyte spheroids as a model system for drug-induced liver injury, liver function and disease. *Sci Rep* **6**, 25187, doi:10.1038/srep25187 (2016).

32 Hu, S. & Monga, S. P. Wnt/-Catenin Signaling and Liver Regeneration: Circuit, Biology, and Opportunities. *Gene Expr* **20**, 189-199, doi:10.3727/105221621X16111780348794 (2021).

33 Oliva-Vilarnau, N. *et al.* Wnt/beta-catenin and NFkappaB signaling synergize to trigger growth factor-free regeneration of adult primary human hepatocytes. *Hepatology*, doi:10.1097/HEP.0000000000000648 (2023).

34 Cancer Genome Atlas Research Network. Electronic address, a. a. d. h. e. & Cancer Genome Atlas Research, N. Integrated Genomic Characterization of Pancreatic Ductal Adenocarcinoma. *Cancer cell* **32**, 185-203 e113, doi:10.1016/j.ccell.2017.07.007 (2017).

35 Jiang, X. *et al.* Inactivating mutations of RNF43 confer Wnt dependency in pancreatic ductal adenocarcinoma. *Proc Natl Acad Sci U S A* **110**, 12649-12654, doi:10.1073/pnas.1307218110 (2013).

36 Wright, S. C. *et al.* FZD5 is a Galphaq-coupled receptor that exhibits the functional hallmarks of prototypical GPCRs. *Sci Signal* **11**, doi:10.1126/scisignal.aar5536 (2018).

37 Jiang, X., Charlat, O., Zamponi, R., Yang, Y. & Cong, F. Dishevelled promotes Wnt receptor degradation through recruitment of ZNRF3/RNF43 E3 ubiquitin ligases. *Molecular cell* **58**, 522-533, doi:10.1016/j.molcel.2015.03.015 (2015).

38 Colozza, G. & Koo, B. K. Wnt/beta-catenin signaling: Structure, assembly and endocytosis of the signalosome. *Development, growth & differentiation* **63**, 199-218, doi:10.1111/dgd.12718 (2021).

39 Bilic, J. *et al.* Wnt induces LRP6 signalosomes and promotes dishevelled-dependent LRP6 phosphorylation. *Science* **316**, 1619-1622, doi:10.1126/science.1137065 (2007).

40 DeBruine, Z. J., Xu, H. E. & Melcher, K. Assembly and architecture of the Wnt/beta-catenin signalosome at the membrane. *Br J Pharmacol* **174**, 4564-4574, doi:10.1111/bph.14048 (2017).

41 Tsutsumi, N. *et al.* Structure of human Frizzled5 by fiducial-assisted cryo-EM supports a heterodimeric mechanism of canonical Wnt signaling. *Elife* **9**, doi:10.7554/eLife.58464 (2020).

42 Angers, S. Frizzled does not get bent out of shape by Wnt. *Sci Signal* **15**, eadd3535, doi:10.1126/scisignal.add3535 (2022).

43 Gratz, L. *et al.* Pathway selectivity in Frizzleds is achieved by conserved micro-switches defining pathway-determining, active conformations. *Nat Commun* **14**, 4573, doi:10.1038/s41467-023-40213-0 (2023).

44 Hauser, A. S. *et al.* GPCR activation mechanisms across classes and macro/microscales. *Nat Struct Mol Biol* **28**, 879-888, doi:10.1038/s41594-021-00674-7 (2021).

45 Xu, L. *et al.* Cryo-EM structure of constitutively active human Frizzled 7 in complex with heterotrimeric Gs. *Cell Res*, doi:10.1038/s41422-021-00525-6 (2021).

46 Schulte, G. & Wright, S. C. Frizzleds as GPCRs - More Conventional Than We Thought! *Trends in pharmacological sciences* **39**, 828-842, doi:10.1016/j.tips.2018.07.001 (2018).

47 Nile, A. H. *et al.* A selective peptide inhibitor of Frizzled 7 receptors disrupts intestinal stem cells. *Nat Chem Biol* **14**, 582-590, doi:10.1038/s41589-018-0035-2 (2018).

48 Nickho, H. *et al.* Developing and characterization of single chain variable fragment (scFv) antibody against frizzled 7 (Fzd7) receptor. *Bioengineered* **8**, 501-510, doi:10.1080/21655979.2016.1255383 (2017).

49 Pavlovic, Z. *et al.* A synthetic anti-Frizzled antibody engineered for broadened specificity exhibits enhanced anti-tumor properties. *MAbs*, 1-11, doi:10.1080/19420862.2018.1515565 (2018).

50 Diamond, J. R. *et al.* Phase Ib clinical trial of the anti-frizzled antibody vantictumab (OMP-18R5) plus paclitaxel in patients with locally advanced or metastatic HER2-negative breast cancer. *Breast Cancer Res Treat* **184**, 53-62, doi:10.1007/s10549-020-05817-w (2020).

51 Neubig, R. R. *et al.* International Union of Pharmacology Committee on Receptor Nomenclature and Drug Classification. XXXVIII. Update on terms and symbols in quantitative pharmacology. *Pharmacological reviews* **55**, 597-606, doi:10.1124/pr.55.4.4 (2003).

52 Changeux, J. P. & Christopoulos, A. Allosteric modulation as a unifying mechanism for receptor function and regulation. *Diabetes Obes Metab* **19 Suppl 1**, 4-21, doi:10.1111/dom.12959 (2017).

53 Eubelen, M. *et al.* A molecular mechanism for Wnt ligand-specific signaling. *Science* **361**, doi:10.1126/science.aat1178 (2018).

54 Schulte, G. & Kozielewicz, P. Structural insight into Class F receptors - What have we learnt regarding agonist-induced activation? *Basic Clin Pharmacol Toxicol*, doi:10.1111/bcpt.13235 (2019).

55 Kozielewicz, P. *et al.* Quantitative Profiling of WNT-3A Binding to All Human Frizzled Paralogues in HEK293 Cells by NanoBiT/BRET Assessments. *ACS Pharmacol Transl Sci* **4**, 1235-1245, doi:10.1021/acsptsci.1c00084 (2021).

56 Wesslowski, J. *et al.* eGFP-tagged Wnt-3a enables functional analysis of Wnt trafficking and signaling and kinetic assessment of Wnt binding to full-length Frizzled. *J Biol Chem* **295**, 8759-8774, doi:10.1074/jbc.RA120.012892 (2020).

57 Wang, C. *et al.* Structural basis for Smoothened receptor modulation and chemoresistance to anticancer drugs. *Nat Commun* **5**, 4355, doi:10.1038/ncomms5355 (2014).

Figures:

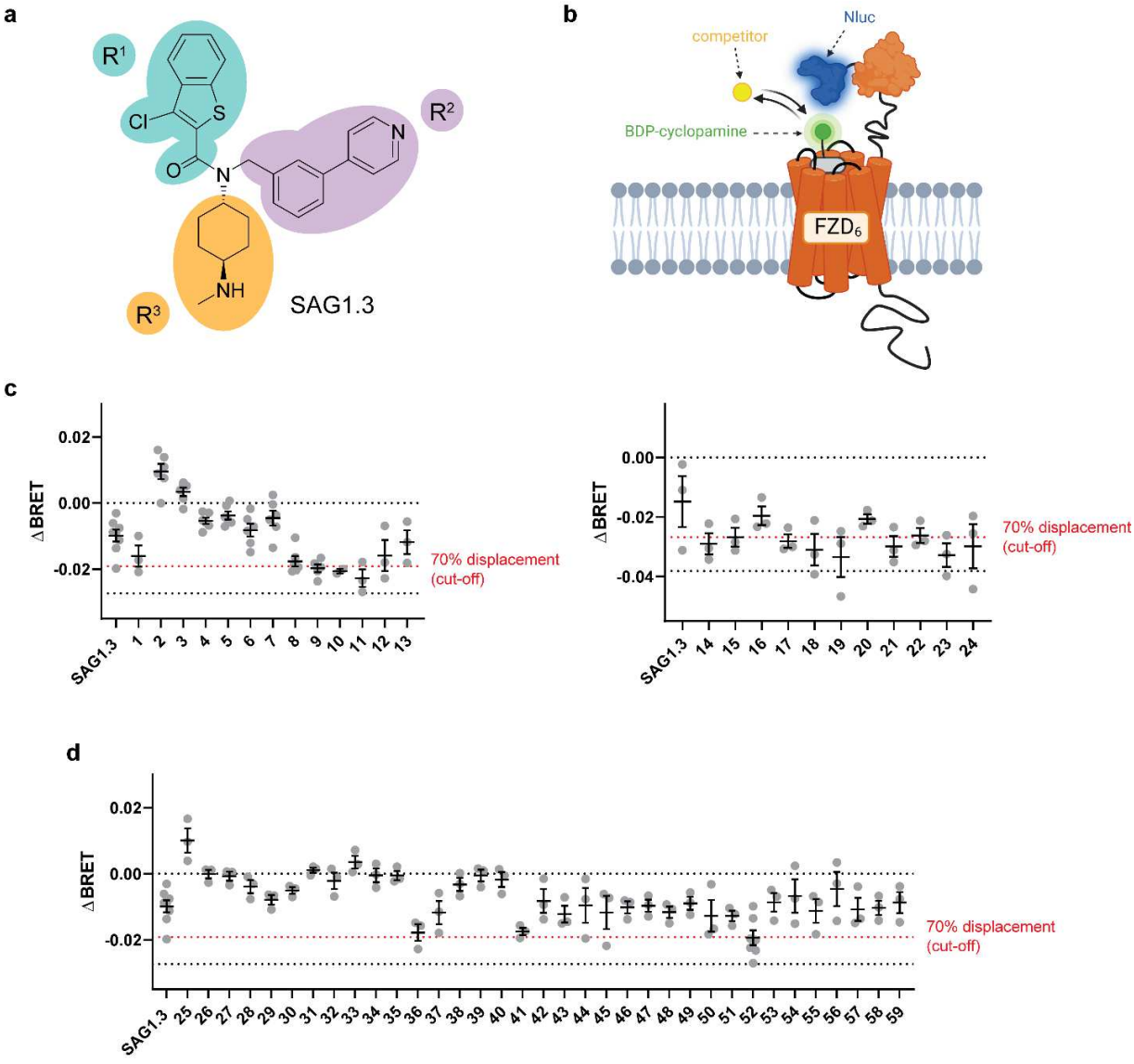

Figure 1. Rationale of the study and screening of SAG1.3 derivatives for binding to Nluc-FZD$_6$.

(**a**) Chemical structure of SAG1.3. The molecule is divided into three regions for subsequent chemical modifications (R^1-R^3). (**b**) Schematic of the BRET-based competition binding assay at Nluc-FZD$_6$ (tracer: BODIPY(BDP)-cyclopamine) used for screening the generated SAG1.3 derivatives. Created with biorender.com. (**c**, **d**) Screening results for SAG1.3 derivatives **1-59**

(10 μM) from BRET-based competition binding assays with BODIPY-cyclopamine (c = 300 nM) performed in ΔSMO HEK293A or ΔFZD_{1-10} HEK293T cells transiently transfected with Nluc-FZD_6. Compounds from the first round of modifications focussing on R^3 (**1**-**24**) are shown in (**c**), while compounds from the second set (**25**-**59**) are shown in (**d**). The lower black dashed line indicates baseline levels ("donor only" conditions) indicative of full tracer displacement. The red dashed line indicates a pre-defined cut-off value (70% tracer displacement), which was used as a decision criterium for further characterization. Note that the absolute ΔBRET values for full displacement in the right panel of (**c**) are different as another plate reader was used for data acquisition. Data in (**c**, **d**) represent mean values ± SEM from 2-8 independent experiments each performed in duplicate.

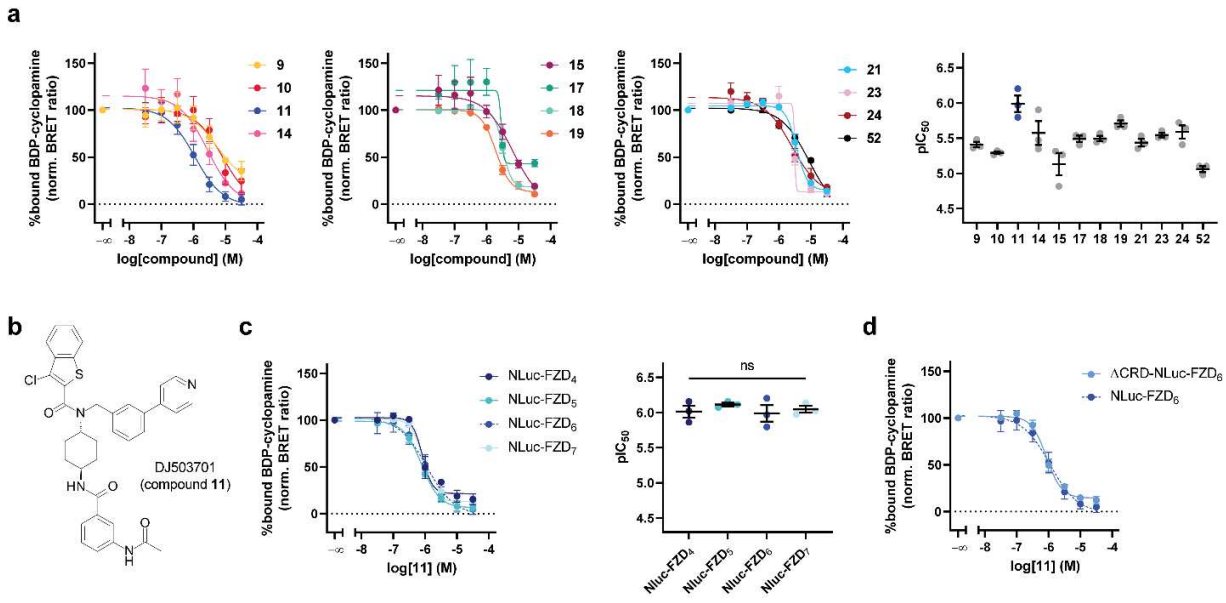

Figure 2. Validation of selected compounds in BRET-based competition binding experiments.

(**a**) Displacement curves and pIC_{50} values from BRET-based competition binding experiments at Nluc-FZD_6 with selected SAG1.3 derivatives and BODIPY-cyclopamine (c = 200 nM). Experiments were performed in ΔFZD_{1-10} HEK293T cells transiently transfected with Nluc-FZD_6. (**b**) Chemical structure of DJ503701 (compound **11**) (**c, d**) Displacement curves and corresponding pIC_{50} values (only in (**c**)) from BRET-based competition binding experiments with compound **11** and BODIPY-cyclopamine (c = 200 nM) performed in ΔFZD_{1-10} HEK293T cells transiently transfected with Nluc-FZD_4, Nluc-FZD_5 or Nluc-FZD_7 (**c**) or ΔCRD-Nluc-FZD_6 (**d**). Note that data for Nluc-FZD_6 (dashed blue lines) in (**c**) and (**d**) were copied from (**a**) for illustration purposes. Experimental data in (**a**, **c** and **d**) represent mean values ± SEM from three independent experiments performed in triplicate. Statistical significance in (**c**) was assessed using one-way ANOVA followed by Tukey's post-hoc test. ns: not significant.

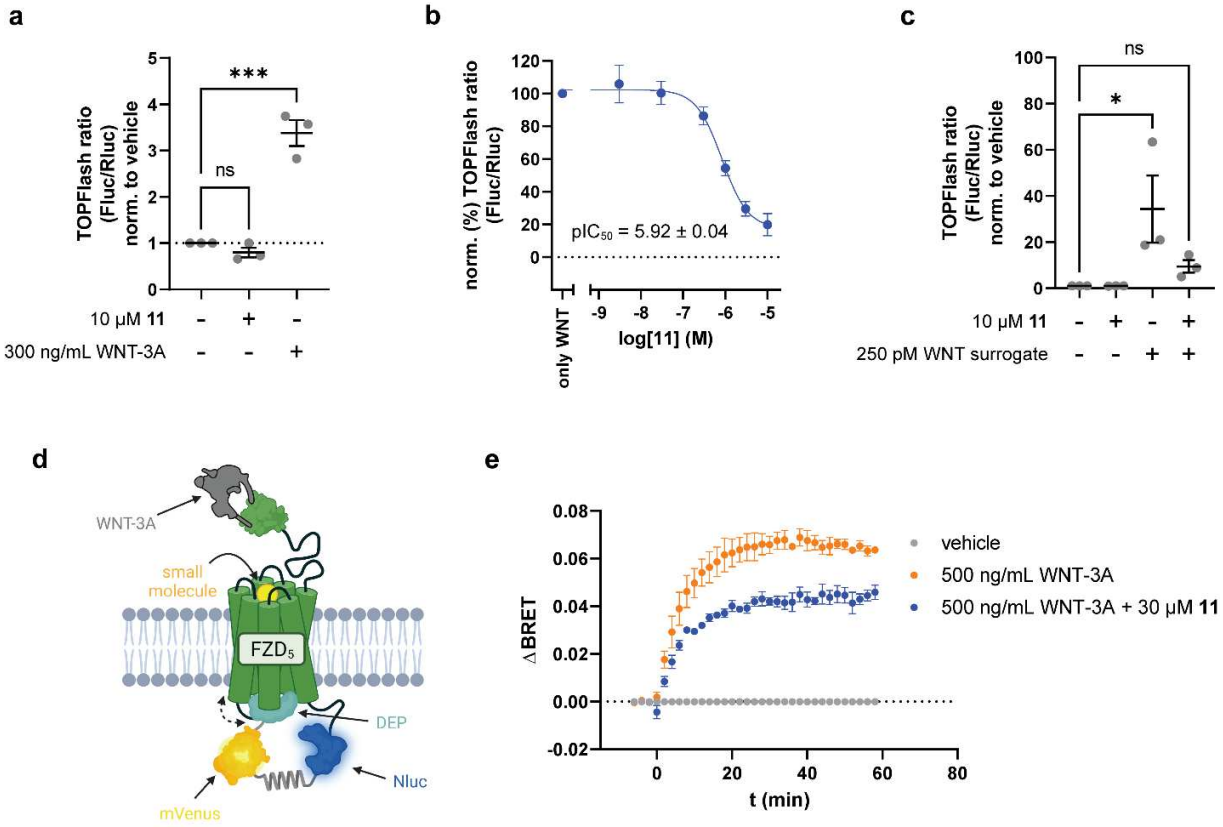

691

692 **Figure 3. Functional characterization of compound 11 defining its mode of action.**
693 (**a**) TOPFlash reporter gene response induced by vehicle control, compound **11** or WNT-3A in
694 ΔFZD$_{1-10}$ HEK293T cells transiently transfected with HiBiT-FZD$_5$. (**b**) Concentration-response
695 curve of compound **11** inhibiting the TOPFlash response induced by 300 ng/mL WNT-3A.
696 Experiments were performed in ΔFZD$_{1-10}$ HEK293T cells transiently transfected with HiBiT-
697 FZD$_5$. (**c**) TOPFlash reporter gene response induced by vehicle control, compound **11**, WNT
698 surrogate or a combination of compound **11** and WNT surrogate in ΔFZD$_{1-10}$ HEK293T cells
699 transiently transfected with HiBiT-FZD$_5$. (**d**) Schematic depiction of the FZD$_5$-DEP-Clamp
700 assay setup. Created with biorender.com. (**e**) Kinetic ΔBRET response of the FZD$_5$-DEP-Clamp
701 sensor recorded upon addition of vehicle control, 500 ng/mL high purity WNT-3A or 500 ng/mL
702 high-purity WNT-3A together with 30 µM of compound **11**. Experiments were performed in

HEK293A cells stably expressing the FZD_5-DEP-Clamp sensor. All experimental data (**a**, **b**, **c** and **e**) represent mean values ± SEM from three independent experiments each performed in triplicate. Statistical significance in (**a**) and (**c**) was assessed using one-way ANOVA followed by Dunnett's post-hoc test. ns: not significant; *: $p < 0.05$; ***: $p < 0.001$.

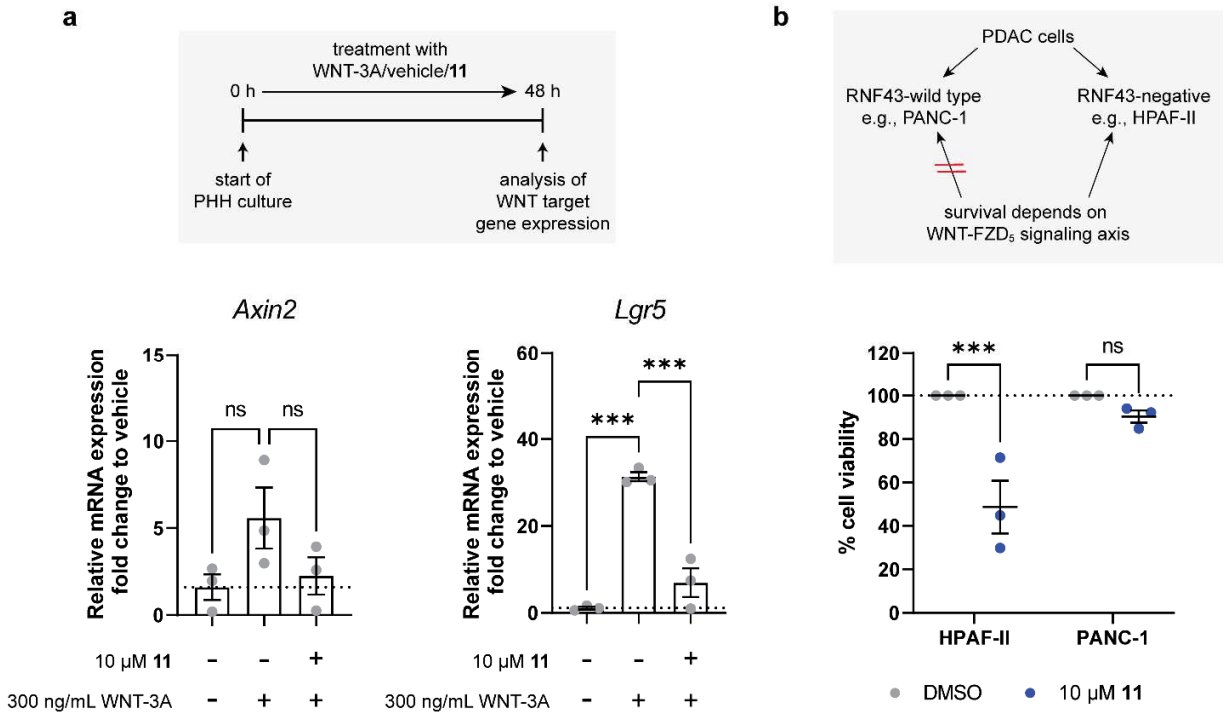

Figure 4. Effect of compound 11 on WNT-induced signaling in primary hepatocyte spheroids and pancreatic cancer cells. (**a**) Effect of compound **11** on WNT-3A-induced gene expression (*Axin2*, *Lgr5*) in primary human hepatocyte (PHH)-derived spheroids. Data shown are mean values ± SEM from three independent experiments. (**b**) Effect of compound **11** or vehicle control on viability of RNF43-negative (HPAF-II) and RNF43-wild type (PANC-1) pancreatic ductal adenocarcinoma (PDAC) cells. Data represent normalized mean values ± SEM from three independent experiments performed in triplicate. Statistical significance in (**a**) was assessed using one-way ANOVA followed by Tukey's post-hoc test, while for (**b**), a two-way ANOVA followed by Šidak's post-hoc test was used. ns: not significant, ***: $p < 0.001$.

Supplementary Files

This is a list of supplementary files associated with this preprint. Click to download.

- Compoundlistfinal.xlsx
- Supplementaryinformationv3GrXXtzandTurkufinal.pdf